Science Advances
AAAS

advances.sciencemag.org/cgi/content/full/4/7/eaas8675/DC1

Supplementary Materials for

Barium isotope evidence for pervasive sediment recycling in the upper mantle

Sune G. Nielsen*, Tristan J. Horner, Helena V. Pryer, Jerzy Blusztajn, Yunchao Shu, Mark D. Kurz, Véronique Le Roux

*Corresponding author. Email: snielsen@whoi.edu

Published 11 July 2018, *Sci. Adv.* **4**, eaas8675 (2018)
DOI: 10.1126/sciadv.aas8675

This PDF file includes:

Precision and accuracy of Ba isotope measurements

Due to the small Ba isotopic variability in our MORB data set it is important to thoroughly assess the associated uncertainties of our Ba isotope measurements. Below we discuss the statistical approach to calculating our measurement precision. Subsequently we also present data for samples measured independently in multiple labs, which support our contention that the data are both precise (± 0.03 ‰) and accurate.

Assessment of Ba isotope measurement precision

Uncertainties were calculated based on the approach described in Horner et al. (2015). Using this method, the long-term uncertainty for sample unknowns is estimated as ± 0.03 ‰ (± 2 SD, standard deviation), a roughly four-fold improvement over previous studies using MC-ICP-MS[53] and similar to uncertainties recently reported for TIMS[23]. Overall, this improvement in uncertainties was achieved by utilizing the Neptune situated in the WHOI Plasma Facility, which affords three key benefits over other MC-ICP-MS approaches:

- Larger dynamic range. This feature permits measurement of large ion beams of ^{138}Ba (≈ 72 %) alongside minor beams from the other isotopes of Ba (all others ≤ 11 %), which is not feasible on some older generation instruments. This feature is particularly important if double spiking, as simultaneous measurement of at least four isotopes is needed. If measuring *m/z* 135→138, one would expect to capture ≈ 97 % of naturally occurring Ba ions in the mass spectrum, whereas *m/z* 134→137 captures only ≈ 28 %.
- Greater mass separation. The Ba mass spectrum is compromised by numerous interferences: Xe (present as an impurity in the Ar carrier gas) at low masses, and La and Ce at high masses (present in samples). The Neptune MC-ICP-MS can simultaneously monitor all masses from *m/z* 131 (Xe) →140 (Ce), though certain instrumental setups cannot. Generally those instruments unable to resolve the entire mass range have omitted ^{138}Ba as this isotope also poses problems associated with dynamic range. Note that thermal ionization mass spectrometry (TI-MS) circumvents this issue entirely as no isobaric Xe is present.
- Higher transmission efficiency. Older generation MC-ICP-MS instruments have ion transmission efficiencies ≈ 2.5 ‰ whereas the Neptune MC-ICP-MS at the WHOI Plasma Facility routinely achieves ≈ 15 ‰ for Ba.

The larger proportion of the Ba mass range sampled by the Neptune coupled to improvements in ion transmission efficiency imply at least a 20-fold improvement in Ba signal intensities compared to older generation MC-ICP-MS instruments. If the sole source of uncertainty were related to ion counting statistics, a 20-fold improvement in signal intensity would result in a four-fold improvement in measurement precision. Thus, based on physical considerations alone, the above analysis suggests that our uncertainty assessment of ± 0.03 ‰ is consistent with uncertainty estimates from existing studies.

Barium-isotopic data are reported as the weighted mean, $x_{mean,}$ of n independent isotopic measurements. Uncertainties are reported as either the ± 2 SD (standard deviation) for sample unknowns, estimated as ± 0.03 ‰ (ref. [22]) or two-times the weighted uncertainty, $\sigma_{\text{mean.}}$,

whichever is larger. The calculation methods for both x_{mean} and σ_{mean} are explained in detail elsewhere[22], but are briefly outlined below.

Mean Ba-isotopic compositions and uncertainties thereof were obtained by 'pooling' the uncertainty from n independent isotopic analyses. The uncertainty on an individual analysis, i, is calculated from the within-run variance (σ_i) about $\delta^{138/134}Ba_{NIST}$ (x_i). This variance is then converted to a weighting, w_i, using

$$w_i = \frac{1}{\sigma_i^2}$$

The weighted mean Ba-isotopic composition, x_{mean}, is then calculated using

$$x_{mean} = \frac{\sum_{i=1}^{n} x_i w_i}{\sum_{i=1}^{n} w_i}$$

The use of weightings is beneficial if σ_i varies between analyses of the same sample. Note that if σ were the same for all samples, σ_{mean} is equivalent to SE, the standard error; i.e., $\sigma/\sqrt{n}$.

The weighted uncertainty, σ_{mean}, is then estimated using

$$\sigma_{mean} = \frac{1}{\sum_{i=1}^{n} w_i}$$

Since σ_i is typically between 0.02 to 0.04 ‰ (± SE) and n between two and four, σ_{mean} is most commonly between 0.01 and 0.02 ‰. Hence, the final uncertainty about x_{mean} is ≤ 0.03 ‰. However, our precision test, demonstrated that our long-term external 2 SD precision is slightly larger at ± 0.03 ‰. Thus, we report all sample uncertainties as either ± 0.03 ‰ or $2\sigma_{mean}$, whichever is greaterNote that the final reported uncertainty is always the larger of 0.03 ‰ and σ_{mean}.

Use of ± 0.03 ‰ (± 2 SD) as our final reported uncertainty is further justified by tests performed with repeat dissolutions and analyses of the $CaCO_3$ powder reference material JCp-1 (ref [22]). This analysis showed that the population variance of x_{mean}—each x_{mean} itself being a weighted mean of three or four independent measurements—was ± 0.03 ‰ (± 2 SD, n = 7). There is thus usually little difference between the long-term 2SD of unknowns and σ_{mean} of a population of individual analyses, which further supports the use of whichever of these two numbers that is the largest. Lastly, analysis of five Ba-depleted surface seawaters showed an even smaller population variance (± 0.02 ‰, 2SD), further supporting that ± 0.03 ‰ is entirely appropriate. Indeed, recent studies of Ba-isotopic compositions in seawater using TI-MS and the same ^{135}Ba—^{137}Ba double spike as previously used at WHOI[22] also report measurement precision of 0.02-0.03 ‰ (refs. [23,28]).

Assessment of Ba isotope measurement accuracy

High precision Ba isotope measurements have only recently been developed and, therefore, there are few reports that enable assessment of accuracy. Here we report Ba isotope compositions for the few international reference materials that have been reported in other studies (table S6). Our results agree exceptionally well with these analyses, which shows that our data are likely accurate as well as precise within the stated uncertainties.

Other potential sources of measurement error

When measuring Ba isotopes there are a number of minor interferences from isotopes of Ce, La and Xe on ^{136}Ba and ^{138}Ba that need to be corrected for[22]. Interferences from isotopes of Xe cannot be avoided as these originate from the Ar used for the plasma that ionizes the sample. We note that measurements of collector backgrounds on-peak (i.e. without deflecting the ion beam away from collector) is not advisable since the Xe signal intensity can vary by as much as a factor of 10 during a two-minute analysis, which could result in erroneous collector background subtractions. We have previously shown that ^{136}Xe interferences to be at a level that allows for highly accurate corrections to be made[22]. Interferences from La and Ce, however, could theoretically be much higher when measuring rock samples than those encountered for seawater samples due to the much higher ratios of Ba to rare earth elements (REEs) in seawater compared with rocks. Our liquid ion exchange chromatography method is specifically designed to separate REEs by eluting Ba in nitric acid, which strongly retains REEs on the resin[54]. As a result we do not observe higher La or Ce ion beams during our rock analyses compared with those found for seawater measurements. On average the ion beam intensities for ^{139}La and ^{140}Ce are at or below 0.02 pA (equivalent to 2mV of signal using 10^{11} Ω resistors), which resulted in corrections on ^{136}Ba and ^{138}Ba signals of <0.05% and <0.01%, respectively. These corrections are negligible compared with those required for ^{136}Xe.

Procedural blanks of Ba added to the sample from reagent blanks and laboratory equipment was monitored throughout this study and were on average 26pg, which is negligible compared with the 50ng of sample Ba processed for all samples. These blanks are similar to our long-term average reagent blank of 15 pg (n = 33), which shows that most of our blank likely originates from reagents rather than laboratory equipment. Given such low levels of contamination, no blank correction is made to the measured Ba-isotopic data.

Barium isotope fractionation at high temperature

There are three principle ways whereby MORB samples can obtain different Ba isotope compositions: 1) Isotope fractionation during melting of isotopically homogenous mantle; 2) Generation of mantle domains with different Ba isotope compositions via Rayleigh distillation during mantle depletion; 3) Addition to the mantle of component(s) with fractionated Ba isotope composition. In the following we discuss in more detail why melting (options 1 and 2) are unlikely to produce any detectable Ba isotope variation.

If Ba isotope fractionation during melting of a homogenous mantle reservoir was the primary explanation for our MORB data then there must be large and systematic variations in degrees of

melting of the DMM. More specifically, it would require that all samples with $\delta^{138/134}$Ba ~ 0.04 and high La/Sm represent lower degrees of melting whereas samples that approach $\delta^{138/134}$Ba ~ 0.14 with lower La/Sm would be generated by gradually higher degrees of melting. However, Ba is a highly incompatible trace element with a bulk partition coefficient during mantle melting of D ~ 0.00012 (ref [17]). Calculations of aggregated fractional melting, which is the dominant melting mode for MORB[56], reveal that >99.9% of all Ba is in the melt after ~1% partial melting. Given that the entire range of MORBs likely represent degrees of melting between 6-20%[40,41], it follows that the net Ba isotope fractionation between the starting mantle composition and the resulting melt will be negligible. This argument also extends to other internal mantle redistribution processes like metasomatism and melt-rock reaction that similarly would be incapable of producing the observed Ba isotope variation.

Often, the DMM has been considered a product of melt depletion through time[41]. Thus, if the residue of mantle melting is isotopically slightly heavier relative to the melt then it is possible to obtain progressively heavier Ba isotope compositions as a function of melt depletion (fig. S2). If these highly depleted mantle domains with heavy Ba isotope compositions then were re-melted to form D-MORB then we would observe the corresponding heavy Ba isotope compositions as a function of prior melt depletion. However, in order to obtain a significantly heavier Ba isotope composition for depleted mantle reservoirs, while at the same time more enriched mantle domains are effectively unfractionated, it is necessary to deplete Ba concentrations by >99.7% of the primitive mantle (fig. S2). Estimates for the most depleted portions of the upper mantle are depleted by ~96.5% compared with the primitive mantle[17]. Therefore, the most depleted parts of the upper mantle need to be depleted by at least an order of magnitude (e.g. 0.3% compared with 3.5% of primitive mantle Ba remaining) more than what is observed in order to obtain the Ba isotope variation we measure in MORB. Another way of looking at this argument is that we would expect MORB samples with $\delta^{138/134}$Ba > 0.1 to register much lower Ba concentrations than samples with $\delta^{138/134}$Ba ~ 0.04 because of the extreme degree of Ba depletion required to generate $\delta^{138/134}$Ba > 0.1 through melt depletion (fig. S2). Although samples with $\delta^{138/134}$Ba > 0.1 generally exhibit low concentrations with an average of ~16 μg/g (table S1 and S2) this value is still higher than almost half the remaining samples in this study that display $\delta^{138/134}$Ba ~ 0.04. Hence, we conclude that the Ba isotope variation in MORB cannot be explained via melt depletion of the upper mantle.

Table S1. Isotope data for MORB glass samples.

Sample name	Lat/Long	Ridge	$^{143}Nd/^{144}Nd^{*}$	$^{87}Sr/^{86}Sr^{*}$	$\delta^{138/134}Ba$	±2SD	*n*	*i*	$^{3}He/^{4}He$ (R_A)	References
AII 107-6 46-1	53.982°S, 3.593°E	SMAR	0.51294	0.70322	0.04	0.03	6	2	8.1	[9,57]
AII 107-7 2-8	46.212°S, 14.073°W	SMAR	*0.512982*	*0.70323*	0.02	0.03	4	1	7.66	[11]
AII 92 31-31a	23.03°N, 44.92°W	NMAR	*0.513177*	*0.70238*	0.12	0.03	6	2	8.07	[10]
AII 93 11-54	24.98°S, 70.012°E	CIR	*0.513066*	*0.70309*	0.04	0.04#	4	1	7.64	[35]
CW 115 37 1D-11	54.598°S, 0.968°W	SMAR	*0.513026*	*0.70304*	0.11	0.03	8	2	7.66	[10]
EN 61 11D-1	9.62°S, 13.23°W	MAR	0.513178	0.70277	0.04	0.03	4	1	5.7	[11,58]
EN0 63 2D-5G	21.5°S, 11.82°W	SMAR	0.513152	0.70237	0.04	0.03	8	2	7.82	[11,58]
ENO 61 13D -1G	10.553°S, 13.007°W	MAR	0.513191	0.70245	0.1	0.03	4	1	7.81	[11,58]
ENO 61 8D-2A g	8.008°S, 13.398°W	MAR	0.513221	0.70237	0.14	0.03	4	1	8.22	[11,58,59]
Juan de Fuca 2	44.61°N, 130.41°W	JdF	*0.513145*	*0.7025*	0.15	0.03	4	1	8.36	[35]
KN162 LEG 7 DREDGE 21-2	53.035°S, 22.468°E	SWIR	*0.513064*	*0.70269*	0.05	0.03	4	1	7.1	[36]
KN162 LEG 7 DREDGE 4-31	52.358°S, 17.113°E	SWIR	*0.512995*	*0.70266*	0.06	0.03	8	2	6.61	[36]
MW 20-1	21°S, 114.19°W	EPR	0.513199	0.70241	0.08	0.04#	4	1	8.25	[60,61]
MW 8712 102-3	13.38°S, 112.33°W	EPR	0.513205	0.70241	0.05	0.03	4	1	9.04	[60,61]
MW 8712 5-3	23.02°S, 114.51°W	EPR	0.513193	0.70239	0.03	0.03	4	1	8.35	[60,61]
TR 89 21D SG-A	38.43°N, 30.36°W	NMAR	0.51298	0.7034	0.03	0.04#	4	1	8$	[35]
TR119 6D-6	35.84°N, 34.18°W	NMAR	0.513122	0.70289	0.05	0.03	8	2	8.04	[10,41]
TR138 1D-3	46.23°N, 27.39°W	NMAR	*0.51302*	*0.70313*	0.06	0.03	4	1	6.93	[10]
TR138 6D-1	50.043°N, 28.933°W	NMAR	0.513226	0.7023	0.14	0.03	4	1	8.04	[10,62]
TR138 8D-1	51.28°N, 30.02°W	NMAR	0.513226	0.70251	0.08	0.03	4	1	8.36	[10,62,63]
TR89 30D-10	39.63°N, 29.74°W	NMAR	0.513033	0.70312	0.02	0.03	4	1	8.07	[10,64]

* - Data in italics from this study, remaining numbers were previously published

- uncertainty of these samples are 2SE. See supplement for details on how errors are reported

$ - Sample had insufficient He for isotope analysis. Value listed here represents average of values obtained for other samples from same mid-ocean ridge segment

n - number of independent isotopic analyses; *i* - replicate sample splits

CIR - Central Indian Ridge; EPR - East Pacific Rise; JdF - Juan de Fuca Ridge; MAR - central Mid Atlantic Ridge; NMAR - Northern Mid Atlantic Ridge; SMAR - Southern Mid Atlantic Ridge; SWIR - South West Indian Ridge

Table S2. Trace element data for MORB glasses in microgram per gram.

Sample name	Sc	V	Cr	Mn	Co	Rb	Sr	Y	Zr	Nb	Cs	Ba	La	Ce	Pr	Nd	Sm	Eu	Tb	Gd	Dy	Ho	Er	Tm	Yb	Lu	Hf	Pb	Th	U
AII 107-6 46-1	40.7	235	370	1256	40	7.25	201	28.4	111	8.96	0.075	*73.9*	8.27	19.6	2.76	12.8	3.71	1.24	0.74	4.58	4.86	1.03	2.88	0.44	2.77	0.41	2.69	0.73	0.785	0.224
AII 107-7 2-8	39.9	284	353	1304	42	2.05	122	32.2	90	2.48	0.02	22.7	3.93	11.3	1.85	9.67	3.31	1.13	0.78	4.41	5.35	1.18	3.32	0.51	3.11	0.49	2.36	0.49	0.254	0.065
AII 92 31-31a	39.7	291	274	1378	42.4	0.6	138	36.7	115	2.23	0.0053	*5.39*	3.75	11.9	2.05	11.1	3.87	1.35	0.92	5.33	6.04	1.31	3.65	0.57	3.54	0.52	2.85	0.47	0.135	0.063
AII 93 11-54	37	274	295	1249	39.1	0.81	99	33.4	84	1.35	0.0078	8.6	2.72	8.91	1.59	8.82	3.26	1.11	0.8	4.5	5.5	1.21	3.4	0.52	3.2	0.49	2.25	0.48	0.11	0.034
CW 115 37 1D-11	40	240	361	1332	44.4	1.73	123	27.4	72	2.36	0.018	18	2.84	8.45	1.41	7.63	2.69	0.98	0.67	3.77	4.51	0.99	2.79	0.43	2.68	0.41	1.86	0.41	0.195	0.053
EN 61 11D-1	40.5	308	186	1437	39.1	8.37	273	34.8	171	18	0.083	99.1	13.4	31.5	4.43	20.5	5.7	1.88	1.01	6.28	6.31	1.29	3.52	0.54	3.19	0.47	4.1	0.94	1.283	0.484
EN0 63 2D-5G	40.7	265	441	1250	43.3	0.23	115	29	76	0.87	0.0024	1.92	2.01	7.09	1.31	7.49	2.84	1.1	0.7	4.1	4.65	1.02	2.86	0.47	2.91	0.41	2	0.33	0.055	0.024
ENO 61 13D -1G	44	287	423	1362	45.6	1.63	90	26.7	55	2.48	0.02	16.7	2.46	6.74	1.12	6.06	2.28	0.87	0.61	3.5	4.1	0.92	2.62	0.44	2.76	0.39	1.5	0.32	0.212	0.069
ENO 61 8D-2A g	40.5	283	326	1298	45.9	2	83	28.5	64	3.59	0.02	21.9	3.28	9.02	1.48	7.96	2.82	0.99	0.69	3.97	4.75	1.05	2.95	0.45	2.87	0.43	1.86	0.32	0.268	0.081
Juan de Fuca 2	46.6	362	95	1631	44	2.08	119	47.8	143	5.1	0.02	19.9	5.64	16.4	2.72	14.4	4.97	1.57	1.18	6.82	7.89	1.74	4.89	0.76	4.7	0.71	3.75	0.7	0.348	0.137
KN162 LEG 7 DREDGE 21-2	36.5	245	361	1180	39.3	0.95	172	29.7	106	2.39	0.01	12.5	3.87	12	2.01	10.6	3.52	1.26	0.76	4.63	5.01	1.09	3.01	0.48	2.86	0.42	2.58	0.65	0.196	0.066
KN162 LEG 7 DREDGE 4-31	41.3	301	325	1457	44.1	5.43	162	40.9	143	8.54	0.061	46.1	7.88	20.1	3.05	15.2	4.86	1.63	1.05	6.24	6.78	1.46	4.05	0.66	3.95	0.58	3.54	0.7	0.809	0.221
MW 20-1	45.5	296	360	1351	39.5	0.46	112	33.3	89	1.2	0.0046	3.83	2.43	8.45	1.54	8.61	3.15	1.15	0.78	4.41	5.35	1.18	3.34	0.52	3.25	0.49	2.24	0.36	0.079	0.029
MW 8712 102-3	45.2	380	101	1636	43.9	1.36	108	43.7	154	2.56	0.016	12.7	3.75	12.1	2.12	11.5	4.18	1.46	1.04	6.22	6.94	1.54	4.35	0.71	4.48	0.64	3.78	0.53	0.205	0.068
MW 8712 5-3	45.7	298	388	1368	43.8	0.24	78	29.3	54	0.48	0.0019	1.07	1.27	4.83	0.97	5.88	2.43	0.96	0.68	3.81	4.69	1.06	3.02	0.5	2.98	0.45	1.62	0.29	0.028	0.013
TR 89 21D SG-A	30.2	290	41	1465	39.2	18.8	269	30.1	152	23.6	0.185	207	18.2	38.9	4.95	20.7	5.02	1.64	0.87	5.49	5.22	1.07	2.9	0.45	2.85	0.41	3.42	1.47	1.984	0.579
TR119 6D-6	42.8	277	158	1362	44.7	3.01	104	25.7	56	4.91	0.03	33.6	4	9.79	1.47	7.3	2.47	0.93	0.6	3.52	4.1	0.92	2.6	0.43	2.75	0.38	1.54	0.35	0.392	0.139
TR138 1D-3	40.3	239	421	1222	40.3	5.34	176	25	74	7.77	0.071	58	6.58	14.5	1.94	8.86	2.7	1.02	0.61	3.67	4.02	0.88	2.48	0.4	2.5	0.36	1.82	0.62	0.887	0.239
TR138 6D-1	40.1	304	217	1408	42.9	1.34	109	42.7	127	2.62	0.015	14	3.67	11.8	2.14	11.9	4.3	1.46	1.04	6.13	6.77	1.49	4.16	0.68	4.18	0.6	3.14	0.54	0.183	0.059
TR138 8D-1	40.2	257	406	1263	41.7	0.99	124	30.2	81	1.95	0.01	11.3	2.57	8.25	1.47	8.21	3.03	1.11	0.73	4.31	4.94	1.1	3.04	0.49	3.02	0.44	2.12	0.3	0.128	0.058
TR89 30D-10	35.7	225	434	1133	41.1	6.11	161	20.9	66	8.22	0.062	73.7	7.18	15.1	2.07	9.18	2.58	0.91	0.53	3.16	3.5	0.75	2.09	0.32	2	0.3	1.66	1.19	0.673	0.205

Table S3. Major element compositions of MORB glasses.

Sample	SiO_2	TiO_2	Al_2O_3	FeO	MnO	MgO	CaO	Na_2O	K_2O	P_2O_5	total	Reference
AII 107-6 46-1	50.98	1.44	15.86	8.88	0.16	7.55	12.16	2.44	0.34	0.16	99.97	[65]
AII 107-7 2-8	50.65	1.33	15.69	9.21	0.17	8.06	11.69	2.54	0.13	0.15	99.62	[65]
AII 92 31-31a	nd	1.67	nd	9.82	0.18	8.26	12.10	nd	nd	0.16	nd	this study
AII 93 11-54	nd	1.33	nd	8.84	0.16	8.15	11.67	nd	nd	0.12	nd	this study
CW 115 37 1D-11	50.54	1.22	15.75	9.81	0.17	7.72	11.28	2.59	0.09	0.11	99.28	[65]
EN 61 11D-1	51.21	2.43	14.35	10.56	0.19	6.14	10.10	3.04	0.53	0.51	99.06	[59]
EN0 63 2D-5G	nd	1.25	nd	8.77	0.16	9.50	13.55	nd	nd	0.10	nd	this study
ENO 61 13D -1G	51.17	0.92	14.97	8.54	0.18	8.55	12.48	2.22	0.09	0.32	99.44	[59]
ENO 61 8D-2A g	nd	1.21	nd	9.35	0.17	8.12	12.34	nd	nd	0.11	nd	this study
Juan de Fuca 2	50.80	1.93	13.80	12.17	0.21	6.83	10.80	2.77	0.22	0.23	99.76	[66]
KN162 LEG 7 DREDGE 21-2	50.84	1.36	16.45	8.13	0.15	8.04	11.43	3.00	0.11	0.12	99.63	[67]
KN162 LEG 7 DREDGE 4-31	50.45	1.85	15.75	9.85	0.19	7.38	10.88	3.18	0.26	0.20	99.99	[67]
MW 20-1	50.20	1.37	14.82	8.66	0.17	7.76	11.75	2.97	0.08	0.12	97.90	[68]
MW 8712 102-3	50.50	1.80	13.90	10.87	0.21	6.80	10.92	2.48	0.12	0.15	97.75	[68]
MW 8712 5-3	50.47	0.98	14.89	8.79	0.18	8.46	12.74	2.13	0.03	0.14	98.80	[68]
TR 89 21D SG-A	50.59	2.00	15.22	10.34	0.19	5.70	10.10	3.06	0.82	0.32	98.34	[69]
TR119 6D-6	51.24	1.06	15.01	9.86	0.18	7.58	12.56	2.26	0.12	0.12	99.99	[65]
TR138 1D-3	nd	1.09	nd	8.27	0.16	8.84	13.33	nd	nd	0.12	nd	this study
TR138 6D-1	51.94	1.65	15.46	9.92	0.18	7.04	10.62	3.06	0.11	0.18	100.16	[65]
TR138 8D-1	51.96	1.18	16.14	8.47	0.16	8.06	11.73	2.82	0.09	0.12	100.73	[65]
TR89 30D-10	50.85	1.10	16.00	8.58	0.15	8.33	12.30	2.11	0.28	0.15	99.85	[65]

nd - not determined

Table S4. Barium isotope data for AOC and sediment core tops.

Latitude;Longitude	Site/Cruise	Core, depth interval	Depth below basement/water depth (m)	[Ba] µg/g	$\delta^{138/134}$Ba	±2sd	n	i
Altered Oceanic Crust								
1.227°N;83.730°W	504B	70R-1, 23-30cm	554.1	0.65	0.12	0.04	4	1
	504B	80R-2, 124-132cm	642.1	1.72	-0.09	0.04	4	1
	504B	82R-2, 26-34cm	659.8	2.91	0.02	0.03	4	1
	504B	82R-3, 9-13cm	664	2.88	-0.03	0.03	4	1
	504B	99R-1, 44-52cm	799.2	1.38	0.15	0.03	4	1
28.984°N; 136.057°E	442B	8-5, 71.5-73.5cm	50.3	15.5	0.07	0.03	6	1
	442B	11-1, 64-66cm	73.4	8.5	0.33	0.03	4	1
	442B	16-1, 81-83cm	121.1	27.7	0.01	0.03	4	1
	442B	17-1, 79-81cm	128.1	11.5	0.29	0.04	4	1
	442B	19-2, 40-42cm	148.2	16.8	0.06	0.03	4	1
25.07°N; 68.05°W	417/418	supercomposite	0-544	nd	0.05	0.03	4	1
Sediments								
6.695°S;130.1117°E	A11-93	24PG, 0-2cm	5106	711	0.00	0.03	4	1
13.0067°S;112.575°E	A11-93	36PG, 0-1.5cm	5467	986	0.04	0.03	5	1
26.8533°S;27.39°W	CHN115	48PG, 1-2cm	5933	488	-0.03	0.04	3	1
20.0933°N;64.575°W	CHN57	2PG, 0-2cm	5808	399	0.00	0.03	4	1
5.3667°N;21.0883°W	EN066	17GGC, 12-13cm	3014	536	0.07	0.03	4	1
2.358°N;19.715°W	EN066	30GGC, 2-4cm	5228	149	0.02	0.03	4	1
60.446°N;20.925°W	EWG9302	18GGC, 0-2cm	2573	276	0.00	0.03	4	1
62.751°N;20.678°W	EWG9302	30GGC, 0-3cm	1188	237	0.03	0.03	4	1
49.902°N; 44.464°W	EWG9302	3GGC, 2-4cm	4082	402	0.03	0.03	4	1
59.067°N;18.016°W	EWG9302	4GGC, 0-2cm	1345	247	-0.02	0.03	4	1
28.9133°N;70.945°W	KNR102	1PG, 0-2cm	5370	436	-0.05	0.04	4	1
28.9567°N;71.1033°W	KNR102	2PG, 0-2cm	5365	430	0.01	0.03	4	1
30.1717°N;69.7733°W	KNR102	4PG, 3-4cm	5300	677	-0.02	0.03	5	1
6.288°N;44.075°W	KNR110	19GGC, 2-3cm	4576	327	0.03	0.03	4	1
4.325°N;43.503°W	KNR110	79GGC, 4.5-6cm	2821	202	0.02	0.03	4	1
28.246°N;74.410°W	KNR140	21GGC, 0-2cm	4705	301	-0.02	0.04	4	1
32.746°N;76.126°W	KNR140	48GGC, 0-2cm	2100	241	0.06	0.03	4	1
32.988°N;76.407°W	KNR140	63GPC, 1-3cm	900	147	0.03	0.03	4	1
26.681°S;46.449°W	KNR159	14GGC, 3-4cm	441	308	0.00	0.06	1	1
25.8823°S;43.3062°W	KNR159	1GGC, 1-2cm	2150	291	0.04	0.03	4	1
29.5362°S;43.3378°W	KNR159	54GGC, 5-7cm	4003	707	0.01	0.03	4	1
5.445°N;77.704°W	KNR176	12GGC, 2-3cm	1845	551	-0.11	0.03	4	1
6.821°N;77.936°W	KNR176	8GGC, 0-2cm	2896	296	0.06	0.03	4	1
51.0608°N;168.0832°E	RNDBT6	12GGC, 4-5cm	3416	2,359	-0.04	0.03	5	1
51.410°N;167.4067°E	RNDBT6	21GGC, 1-2cm	2727	1,155	-0.04	0.03	5	1
51.1067°N;167.8283°E	RNDBT6	3GGC, 5-7cm	2610	2,412	-0.04	0.03	5	1
10.0328°N;65.0842°E	TN041	21PG, 0-2cm	4426	595	0.08	0.05	2	1
17.201°N;59.9502°E	TN041	31PG, 4-5cm	2935	812	0.03	0.03	5	1
17.746°N;57.482°E	TN047	14GGC, 6-7cm	594	132	0.03	0.03	4	1
19.232°N;58.518°E	TN047	21GGC, 7-8cm	1257	290	0.03	0.03	4	1
15.967°N;61.474°E	TN047	2GGC, 8-9cm	3989	1,188	0.02	0.03	4	1

n - repeat isotope analyses; i - number of individual sample splits processed

Table S5. Partition coefficients used to calculate sediment melting.

Element	melt-solid partition coefficient
Ba	1.6
Rb	2.2
Sr	7.5
Nb	1.4
La	0.55
Ce	0.56
Nd	0.40
Sm	0.28
Pb	5
Th	0.75

Values calculated based on data in Hermann and Rubatto[43]

Table S6. Barium isotope data for international reference materials.

NIRVANA Labs (this study)					Literature		
Standard	$\delta^{138/134}Ba_{NIST}$	± 2 SD	*n*	*i*	$\delta^{138/134}Ba_{NIST}$	± 2 SD	Reference
BHVO-1 (USGS)	+0.04	0.03	9	2	+0.05	0.04	[70]
G-2 (USGS)	+0.04	0.03	17	4	+0.03	0.04	[70]
JA-2 (GSJ)	+0.04	0.03	4	1	+0.04	0.05	[71]
JCp-1 (GSJ)	+0.27	0.03	31	5	+0.29	0.03	[22]

n - number of independent isotopic analyses; *i* - replicate sample splits

USGS - US Geological Survey; GSJ - Geological Survey of Japan

Figure captions:

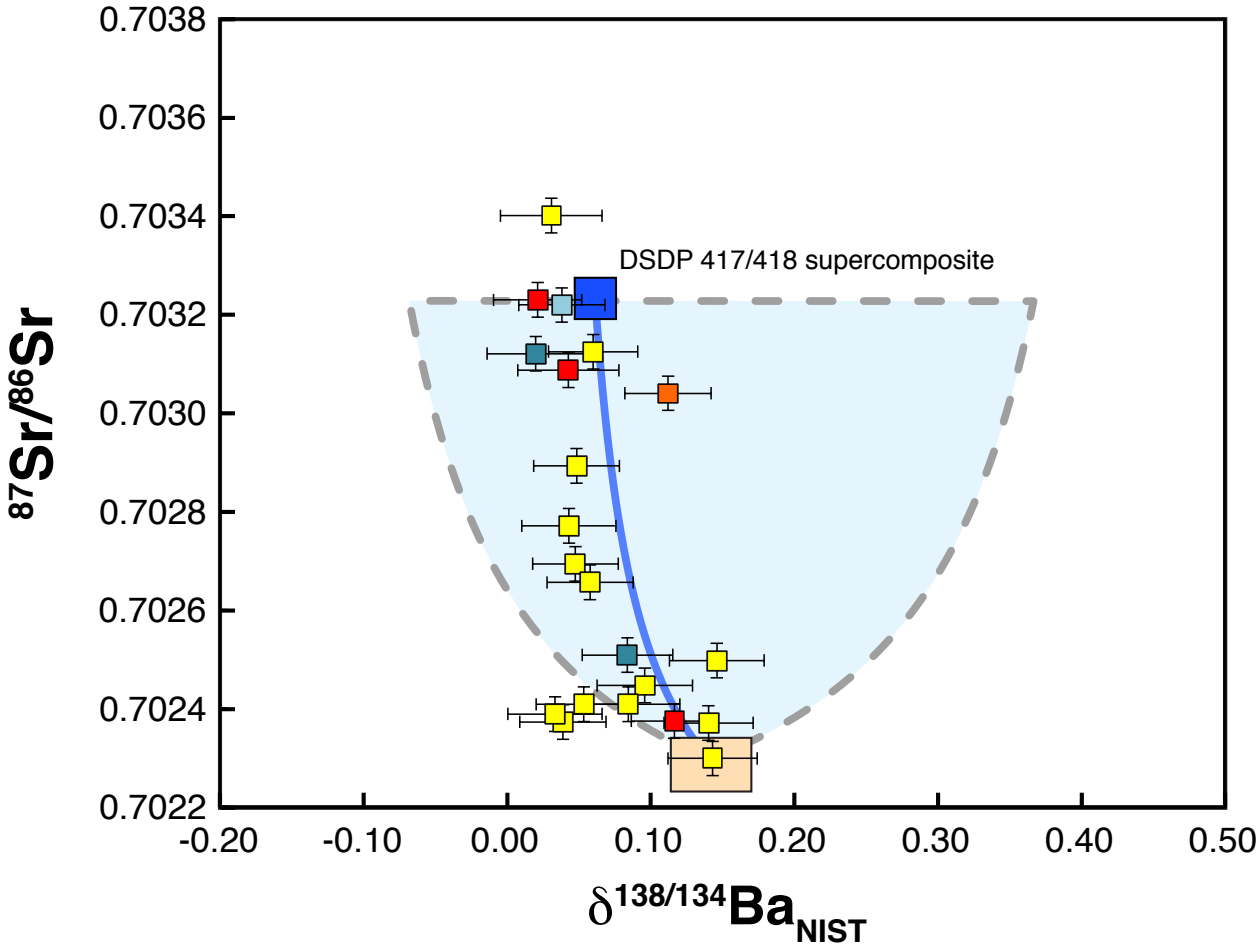

Fig. S1. Barium isotopes plotted against Sr isotopes for MORB samples. Also shown is a mixing field between DMM (light brown square) and the range of AOC compositions observed (table S4 and ref. 34). An additional mixing line is also shown between DMM and the DSDP 417/418 supercomposite (bold blue line).

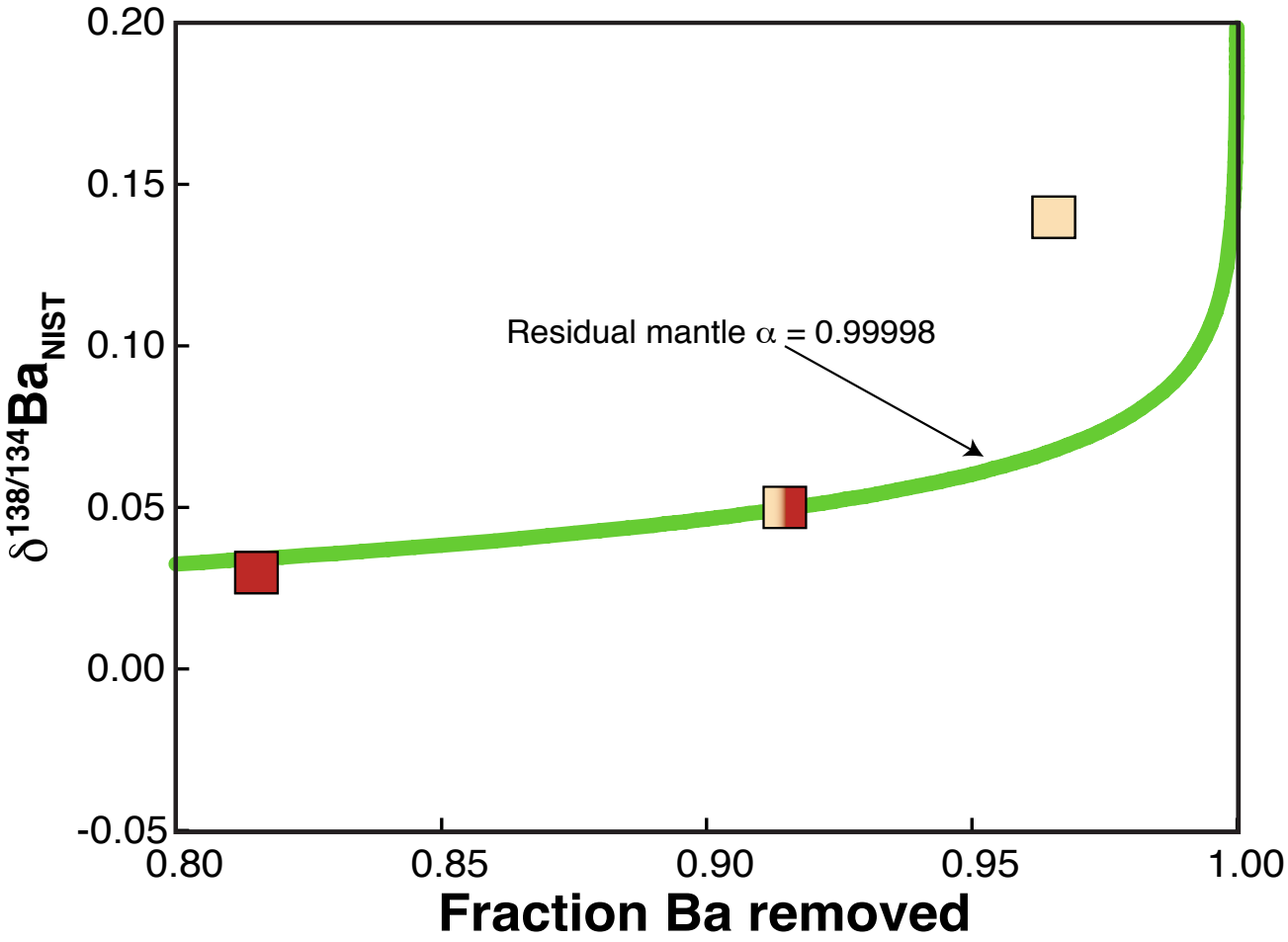

Fig. S2. Calculated Ba isotope variation in MORB mantle reservoirs generated by hypothetical isotope fractionation during melt depletion. The calculation assumes that Ba is removed from the primitive pyrolite mantle [Ba] = 6.6 μg/g[55] that had an arbitrary starting composition of $\delta^{138/134}$Ba = 0. The three data points represent the mantle reservoirs of E-MORB (dark red), N-MORB (graded pale, dark red) and D-MORB (pale). These three mantle reservoirs have been estimated to contain 1.219 μg/g, 0.563 μg/g and 0.227 μg/g Ba[17], which corresponds to 81.5%, 91.5% and 96.5% Ba depletion relative to pyrolite.